Search for biaxiality in a shape-persistent bent-core nematic liquid crystal

Young-Ki Kim,[a] Madhabi Majumdar,[b] Bohdan I. Senyuk,[a] Luana Tortora,[a] Jens Seltmann,[c] Matthias Lehmann,[c,d] Antal Jakli,[a] Jim T. Gleeson,[b] Oleg D. Lavrentovich*[a] and Samuel Sprunt*[b]

[a]*Chemical Physics Interdisciplinary Program and Liquid Crystal Institute, Kent State University, Kent, OH 44242, USA. E-mail: olavrent@kent.edu*
[b]*Department of Physics, Kent State University, Kent, OH 44242, USA.*
E-mail: ssprunt@kent.edu
[c]*Institute of Chemistry, Chemnitz University of Technology, 09107 Chemnitz, Germany*
[d]*Institute of Organic Chemistry, Julius-Maximillians-Universiät Würzburg , 97074 Würzburg , Germany*

Using a range of optical techniques, we have probed the nature of orientational order in a thermotropic bent-core liquid crystal, which features a shape-persistent molecular architecture designed to promote a biaxial nematic phase. In the upper range of the nematic phase (enantiotropic regime), dynamic light scattering reveals strong fluctuations attributable to the biaxial order parameter, in addition to the usual uniaxial director modes. Assuming a Landau-type expansion of the orientational free energy, we estimate the correlation length associated with these fluctuations to be ~100 nm. At lower temperatures, and mainly in the monotropic regime of the nematic, we observe by optical conoscopy an apparently biaxial texture, which develops when the sample temperature is changed but then relaxes back to a uniaxial state over time scales much longer than observed in the light scattering measurements. A combination of fluorescence confocal polarizing microscopy and coherent anti-Stokes Raman scattering confirms that the conoscopic texture arises from a flow-induced reorientation of the molecules, associated with a large thermal expansion coefficient of the material, rather than from the spontaneous development of a macroscopic secondary optical axis. We discuss a model to account for the observed behavior at both high and low temperatures based on the temperature-dependent formation of nanoscale, biaxially ordered complexes among the bent-core molecules within a macroscopically uniaxial phase.

I. Introduction

The development of mesogenic molecules with reduced symmetry shapes and stable nematic phases has reinvigorated the historical quest in thermotropic liquid crystals for the optically biaxial fluid phase predicted by Freiser in 1970.[1] Nematics formed from bent-core molecules (BCNs) have been a major focus of this renewed attention, since the "bow" shape of these mesogens naturally specifies a secondary direction for orientational ordering, which is orthogonal to the average long molecular axis – *i.e.*, to the primary or uniaxial director $\vec{\boldsymbol{n}}$. So far, however, an impressive range of recent studies[2-27] has drawn disparate conclusions on the issue of biaxiality, while nevertheless exposing various interesting phenomena and properties associated with certain BCNs.[28-30]

In this paper, we investigate the possibility of biaxiality in a BCN, which incorporates a shape-persistent core architecture designed to promote the development of a secondary axis for orientational order. The non-symmetrically substituted thiadiazole,[26] whose chemical structure (abbreviated DT6Py6E6) is shown in Fig. 1, contains extra hydrocarbon chains attached at similar ring positions on each arm of the core. These lateral chains stabilize the nematic phase over a wide range, encompassing an enantiotropic region (90-154 ^{o}C) and a monotropic regime that extends on cooling down to ambient temperature. Our study employs dynamic light scattering, which can selectively probe fluctuations of biaxial orientational order in a uniaxial phase, and various types of microscopy including optical conoscopy, fluorescence confocal polarizing microscopy (FCPM),

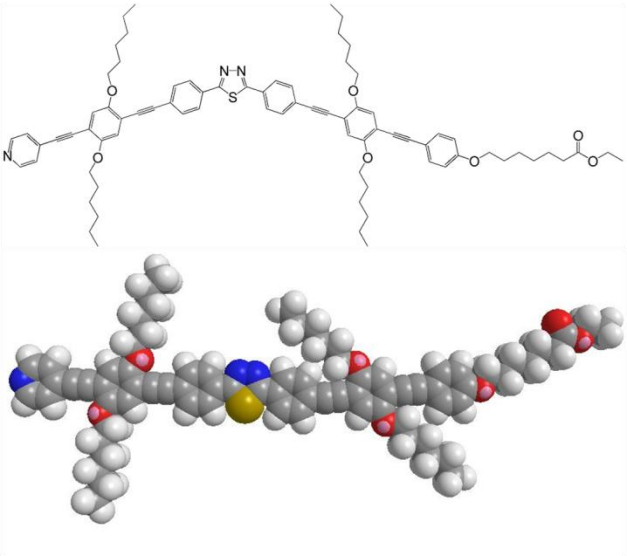

Fig. 1 Chemical structure and space filling model of the bent-core liquid crystal DT6Py6E6.

and coherent anti-Stokes Raman scattering (CARS) microscopy. In combination, the microscopy techniques effectively discriminate the optical texture of a true biaxial state from various distortions in the alignment of the uniaxial director in nematic samples.

Our results are summarized as follow. At higher temperatures (enantiotropic regime), we detect significant light scattering from a nonhydrodynamic mode, which, as the scattering selection rules for the sample geometry utilized imply, arises from fluctuations of the biaxial order parameter in the uniaxial phase. The orientational correlation length associated with these fluctuations is estimated to be ~100 nm, and increases (but not critically) with decreasing temperature within the enantiotropic range. For lower temperatures (mainly in the monotropic range), we observe a conoscopic figure that suggests a biaxial phase, yet we find that the characteristic "biaxial" splitting of isogyres is transient in nature and results from a tilt of the uniaxial director, which in homeotropically oriented samples mimics the conoscopic texture of a biaxial phase. The tilt is triggered by a change in temperature T and a significant thermal contraction/expansion of the material, which induces a flow that reorients the molecules.

We will argue that the two main observations short-range biaxiality fluctuations at fixed T and flow-induced tilt of the uniaxial director while changing T – originate from a temperature –dependent, biaxial complexing of molecules within the macroscopically uniaxial nematic. The notion of such complexes, which may differ from the traditional "cybotactic" nematic groups[32] in that they are not simply pretransitional fluctuations in smectic order, is now new. Theoretical studies have explored via Landau expansion the consequences of separate order parameters describing the density of biaxial "complexes" of some average size and their macroscopic ordering ("phase" biaxiality).[31] Experimentally, small angle X-ray scattering (SAXS) studies[7-12] of several BCNs reveal smectic-C-type short-range molecular configurations, even when there is no nearby smectic phase. Moreover, other SAXs measurements[26] clearly indicates molecular complexing in the nematic phase of DT6Py6E6, although this is apparently not of the smectic-C-type.

II. Light scattering background

In this section, we briefly review essential theoretical results motivating our design of light scattering experiments to probe for biaxial fluctuations. In a uniaxial nematic phase, one may anticipate a contribution due to overdamped fluctuations of the biaxial order parameter, in addition to the usual overdamped director modes.[33] The biaxial order parameter is a symmetric, traceless, second rank tensor ξ_{ij}, whose components, defined in the plane perpendicular to $\vec{\boldsymbol{n}} = \vec{z}$, are $\xi_{xx} = -\xi_{yy}$, and $\xi_{xy} = \xi_{yx}$.

To lowest (quadratic) order, the fluctuations of $\vec{n}$ and ξ_{ij} decouple in the Landau-deGennes expression for the nematic free energy.[34] Then, the mean square amplitude of the $\vec{n}$ fluctuations may be calculated in the standard way from the elastic free energy for a uniaxial nematic.[33] For the depolarized, homeotropic scattering geometry depicted in Fig. 2, with the incident (scattered) polarization perpendicular (parallel) to the horizontal scattering plane containing the average $\vec{n}$ (VH geometry), the intensity of the director scattering arises strictly from a combination of twist and bent elastic distortions of $\vec{n}$, and is given by,

$$I_{\mathrm{VH},\vec{n}} \propto \frac{\left(\Delta\varepsilon_u\right)^2 G_{\mathrm{VH},\vec{n}} K_{\mathrm{B}} T}{K_{22} q_{\perp}^{\ 2} + K_{33} q_z^{\ 2}} \tag{1}$$

Here $\Delta\varepsilon_u = \varepsilon_{zz} - \left(\varepsilon_{xx} + \varepsilon_{yy}\right)/2$ is the saturated dielectric anisotropy of the uniaxial nematic a the appropriate (optical) wavelength, K_{22} and K_{33} are the Frank elastic constants corresponding of bend and twist distortions of $\vec{n}$, and $q_z\left(q_{\perp}\right)$ is the component of the scattering vector along (perpendicular to) the average director. In eq (1), the optical factor $G_{\mathrm{VH},\vec{n}}$, which incorporates the polarization selection rules for the scattering,[33] is given by

$$G_{\mathrm{VH},\vec{n}} = \frac{n_{\|}^{\ 2} \sin^2\left(2\theta - \theta_i\right)}{n_{\perp}^{\ 2} n_{\|}^{\ 2} + \left(n_{\|}^{\ 2} - n_{\perp}^{\ 2}\right)\sin^2\left(2\theta - \theta_i\right)} \tag{2}$$

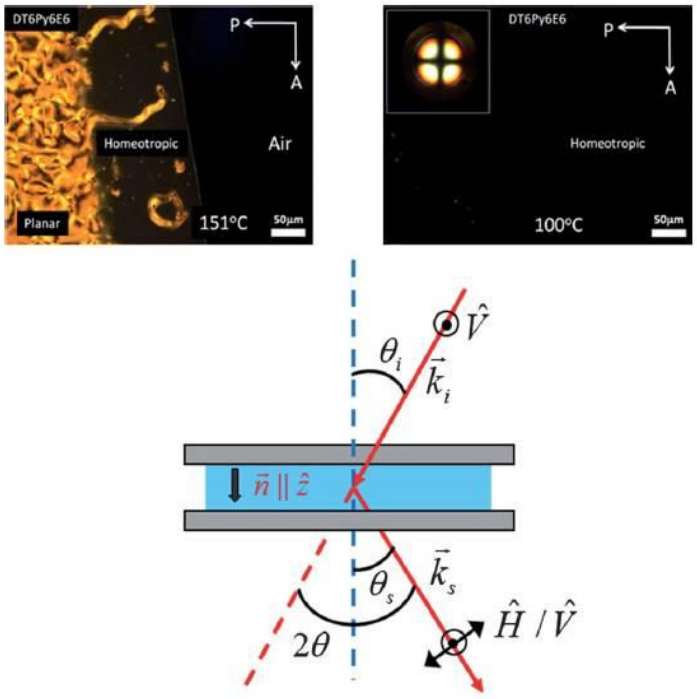

Fig. 2 Top: polarizing microscope texture of DT6Py6E6 sample used in the light scattering experiment, showing the transition from the isotropic phase to a well-aligned, homeotropic nematic state. (The conoscopic figure inset in the image on the right indicates that the nematic is uniaxial over the temperature range studied.) Bottom: light scattering geometry used to detect biaxial order parameter fluctuations in the uniaxial state. Polarized (VV) scattering and the setting $2\theta = \theta_i$ in depolarized (VH) scattering correspond to "dark" uniaxial conditions where, theoretically, the $\vec{n}$ director scattering should vanish.

The angle θ_i is the in incident angle of the light measured in the laboratory frame away from the sample normal, and 2θ is the detection angle measured from the incident light direction (Fig. 2). The quantities $n_{\|}$, $n_{\perp}$ are the principal refractive indices of the uniaxial phase. In the polarized (VV) scattering geometry, which was also studied in our experiment, the cross-section for the director modes theoretically vanishes,

$$G_{\mathrm{VV},\vec{n}} = 0 \text{ and } I_{\mathrm{VV},\vec{n}} = 0 \tag{3}$$

From the hydrodynamic theory for a uniaxial nematic, the relaxation rate for the twist-bend director mod is,

$$I_{\vec{n}}\left(\vec{q}\right) = \frac{K_{22}{q_{\perp}}^2 + K_{33}{q_z}^2}{\eta_2\left(\vec{q}\right)} \tag{4}$$

where $\eta_2\left(\vec{q}\right)$ is a $\vec{q}$-dependent combination of the five independent viscosities characterizing a nematic fluid.[33]

Next, we turn to scattering from biaxiality fluctuations. The connection between the nematic dielectric tensor and the biaxial order parameter[35] implies that the depolarized and polarized scattered intensities at scattering vector $\vec{q}$ are proportional to the mean square amplitudes of the Fourier components $\xi_{if}\left(\vec{q}\right) = \xi_{fi}\left(\vec{q}\right)$, where *i*, *f* refer to the incident and scattered polarization directions, respectively. These amplitudes may be calculated from a Landau expansion of the free energy in the invariants of the order parameter and its gradients; to quadratic order one has;[34]

$$F_{\xi} = \frac{1}{2}\int \mathrm{d}V\left[a\xi_{ij}\xi_{ij} + C_{\|}\left(n_k\nabla_k\xi_{ij}\right)\left(n_l\nabla_i\xi_{ij}\right) + C_{\perp}\left(\delta_{kl} - n_k n_l\right)\times\left(\nabla_k\xi_{ij}\right)\left(\nabla_l\xi_{ij}\right)\right]$$

In this expression, the coefficient *a* contains the temperature dependence that drives a uniaxial to biaxial transition, while the ratio of the temperature independent coefficients $C_{\perp}$ and $C_{\|}$ to a determines two orientational correlation lengths for biaxial order, $l_{\|} = \sqrt{C_{\|}/a}$ and $l_{\perp} = \sqrt{C_{\perp}/a}$. The symbol δ_{kl} represents the Kronecker delta function, and summation on the indices $\left(i,j,k,l\right) = \left(x,y,z\right)$ is implied.

Fourier analysis of this free energy density (with $\vec{n} = \vec{z}$) and use of the equipartition theorem then imply the following contribution to the scattered intensity due to biaxiality fluctuations,

$$I_{if,\xi} \propto \frac{\left(\Delta\varepsilon_b\right)^2 G_{if,\xi} K_{\mathrm{B}} T}{a + C_{\|}{q_z}^2 + C_{\perp}{q_{\perp}}^2} \tag{5}$$

where $\Delta\varepsilon_b = \varepsilon_{yy} - \varepsilon_{xx}$ is the maximum (saturated) dielectric anisotropy arising due to biaxiality (*e.g.*, if all the "bow" directions of the bent-core molecules lie in either the *x* or *y* direction). The optical factors for the homeotropic scattering geometry (Fig. 2) are,

$$G_{\mathrm{VH},\xi} = \frac{{n_{\perp}}^2\left[{n_{\|}}^2 - \sin^2\left(2\theta - \theta_i\right)\right]}{{n_{\perp}}^2{n_{\|}}^2 + \left({n_{\|}}^2 - {n_{\perp}}^2\right)\sin^2\left(2\theta - \theta_i\right)},\ G_{\mathrm{VV},\xi} = 1 \tag{6}$$

Using a simple Landau-Khalatnikov equation to describe the diffusive relaxation of fluctuations in ξ_{ij} (and assuming an isotropic viscosity η_ξ), we get the relaxation rate,

$$\Gamma_\xi(\vec{q}) = \frac{a + C_\parallel q_z^{\,2} + C_\perp q_\perp^{\,2}}{\eta_\xi} \tag{7}$$

The fluctuation in ξ are nonhydrodynamic, with a cut-off in mean square amplitude and a gap in relaxation rate at small q proportional to the coefficient a in the free energy. This fact, together with the expectation that $(\Delta\varepsilon_b)^2 \ll (\Delta\varepsilon_u)^2$, means the scattering cross-section for biaxiality fluctuations should be much weaker than that for the ordinary uniaxial director modes (except in the immediate vicinity of a uniaxial to biaxial transition, where $a \to 0$). Therefore, in order to probe the biaxial mode, scattering experiments must access geometries where the standard uniaxial director modes are "dark". The homeotropic sample alignment, used in our experiments, offers two convenient "dark" geometries: For VH scattering, the condition $2\theta \approx \theta_i$ should minimize the director scattering [$G_{\mathrm{VH},\vec{n}} \approx 0$ in eqn (2)], and a mixture of director and order parameter fluctuations should be observed when moving off this minimum. In the VV geometry, the scattering from $\vec{n}$ fluctuations should be extinguished for all 2θ [eqn (3)]. Both geometries where utilized in our light scattering experiments.

III. Sample preparation and experimental details

The bent-core compound DT6Py6E6 (Fig. 1) was synthesized as described in ref. 26. In cooling, at a rate of $1\,^{\circ}\mathrm{C\,min^{-1}}$, the nematic phase range is $< 20\,^{\circ}\mathrm{C}$ to $154\,^{\circ}\mathrm{C}$. However, in the monotropic regime ($\leq 90\,^{\circ}\mathrm{C}$) and specifically below $50\,^{\circ}\mathrm{C}$, we observed that the material typically crystallizes in ~6 h. We therefore performed all our low-temperature experiments within a few hours. The experimental cells for our studies were assembled from parallel glass plates spin-coated with a thin layer of the passive inorganic material NHC AT720-A (Nissan Chemical Industries, Ltd.) to produce alignment of optic axis (director) $\vec{n}$ perpendicular to the surfaces of the plates (homeotropic alignment). The gap between the plates was set by glass spacers mixed into UV epoxy (Norland Optical Adhesive 65, Norland Products, Inc.) that was used for sealing the cell edges. The cell gap was measured by optical interference. The LC material was filled into the cells by capillary action at temperatures above the clearing point (T_{NI}). For the conoscopic, FCPM, and CARS studies, the sample temperature was maintained within $0.01\,^{\circ}\mathrm{C}$ using a commercial hot-stage (LT350, Linkam Scientific Instruments) and controller (Linkam TMS94). Two homeotropic samples of DT6Py6E6, with 4.9 and 23 μm thicknesses, were prepared for light scattering, and housed in a temperature-controlled oven with optical access and millidegree stability.

Fig. 2 shows a typical example of the uniform dark texture observed by polarizing optical microscopy (with crossed polarizer/analyzer), after cooling a sample from the isotropic to enantiotropic nematic state and allowing the sample temperature to equilibrate. The dark texture indicates excellent homeotropic nematic alignment, while the fourfold symmetric conoscopic figure shown in the inset is consistent with a uniaxial phase.

In the light scattering experiment, laser radiation ($\lambda_0 = 633\,\mathrm{nm}$) was incident on the samples at lab angle $\theta_i = 25^{\circ}$ and polarized normal to the horizontal scattering plane containing the uniaxial director $\vec{n}$, while the

scattered light, polarized either in the plane or vertical to it, was collected at various angles 2θ. The relative fluctuation amplitudes and the relaxation rates of the observed fluctuation modes are extracted from analysis of the time correlation function, $g(\tau)=\langle I(t)I(t+\tau)\rangle/\langle I(t)\rangle^2$, of the scattered light intensity I. The correlation function was measured in the homodyne regime using standard instrumentation. (The angled brackets denote a time average, equivalent to an ensemble average when very many spatial correlation volumes are sampled.) Our typical procedure was to measure $g(\tau)$ as a function of 2θ at fixed temperature T below T_{NI}, and then repeat the measurements at lower temperatures.

IV. Results: light scattering

We turn first to the results of light scattering measurements conducted in the enantiotropic regime

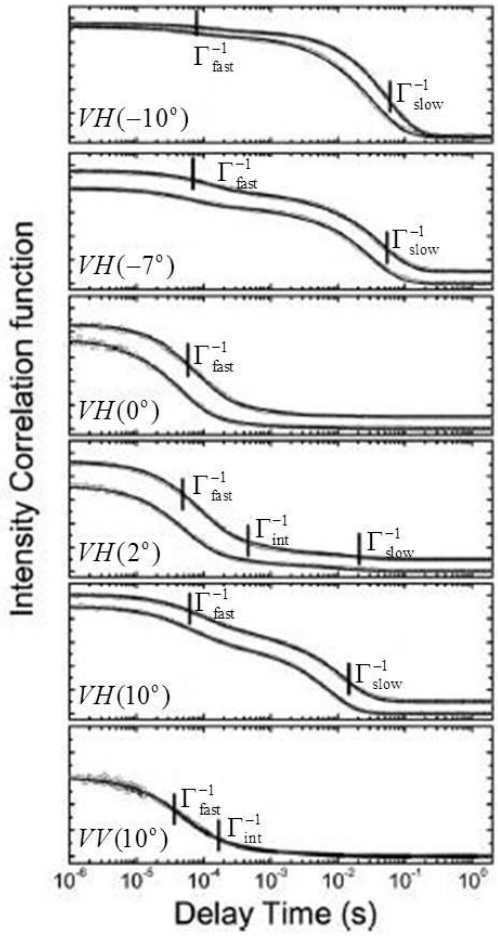

Fig. 3 Upper panels: representative time correlation functions of the depolarized (VH) scattered intensity recorded on thin ($4.9\,\mu m$, upper curves) and thick ($23\,\mu m$, lower curves) homeotropic samples of DT6Py6E6 at a temperature $25\,^{o}C$ below T_{NI}. The data are displayed for various values of $2\theta-\theta_i$ (in parentheses), and the correlation amplitude to background ratio is ≥ 0.9 (homodyne limit). Solid lines through the data represent fits of the data to a sum of exponential decays (see text). Bottom panel: a correlation function recorded on the $4.9\,\mu m$ sample for polarized (VV) scattering. Decay times of the modes are indicated by the inverse relaxation rate (Γ^{-1}).

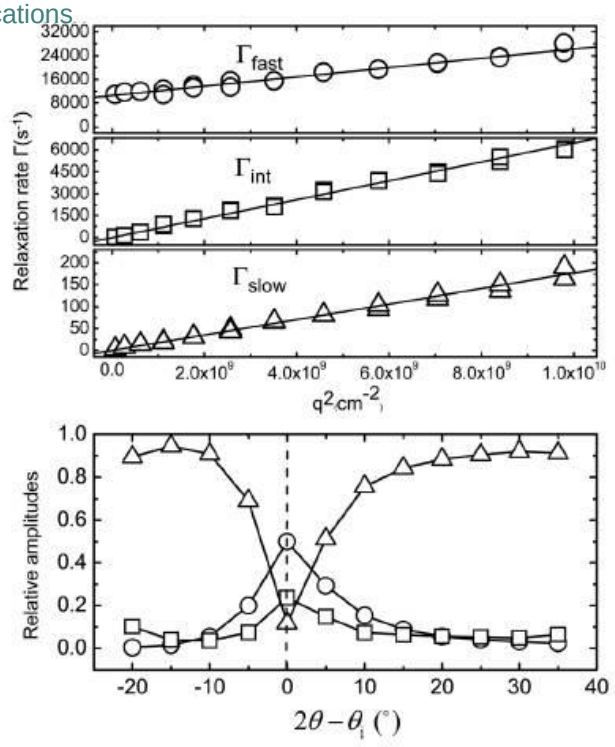

Fig. 4 Upper panels: dispersion of the relaxation rates of the three modes detected in the uniaxial nematic phase of the 4.9μm DT6Py6E6 sample (with $T_{NI}-T=33\,^{\circ}\mathrm{C}$). The slowest mode (Γ_{slow} , triangles) is the hydrodynamic twist-bend mode of the $\vec{n}$ director, while the fast mode (Γ_{fast} , circles) is identified with nonhydrodynamic fluctuations of the biaxial order parameter. The intermediate mode (Γ_{int} , squares) is relative mode amplitudes as a function of $2\theta=\theta_i$ (4.9μm sample, VH scattering geometry, $T_{NI}-T=33\,^{\circ}\mathrm{C}$). The slow mode shows a sharp minimum, and the fast mode a corresponding peak, at $2\theta=\theta_i=0$ (the "dark" uniaxial condition), while the intermediate mode scatters rather weakly for all 2θ .

($90\le T<154\,^{\circ}\mathrm{C}$); these are summarized in Fig. 3-5. The top plots in Fig. 3 show typical VH correlation data recorded for various 2θ angles to either side of and including the value corresponding to the "dark uniaxial" condition, $2\theta=\theta_i=25^{\circ}$. Above and below this value, the relaxation of two distinct fluctuation modes is clearly observed, with the relaxation rate (Γ_{slow}) of the slower mode decreasing, and its relative amplitude increasing, for smaller 2θ (*i.e.*, for scattering wavenumber $q\to 0$). These features are consistent with eqn (1) and (4) for the hydrodynamic twist-bend fluctuations of the uniaxial director. At the value $2\theta=\theta_i$, the contribution of the director mode drops sharply, as expected from eqn (3). On the other hand, the faster mode (relaxation rate Γ_{fast}) is observed for all values of 2θ, and it dominates the scattering in the "dark uniaxial" condition. This behavior, combined with the relatively weak variation of Γ_{fast} with 2θ (indicative of a non-hydrodynamic mode), agrees with the predictions of eqn (5) and (7) for biaxial order parameter fluctuations.

In fact, a quantitative analysis of the correlation data reveals an additional, weakly scattering mode with a relaxation rate (Γ_{int}) *intermediate* between Γ_{slow} and Γ_{fast}. As indicated in Fig. 3, its presence can be seen in the data for $2\theta=\theta_i$. Moreover, even for $2\theta\simeq\theta_i$, we still detected a small contribution of the uniaxial director mode,

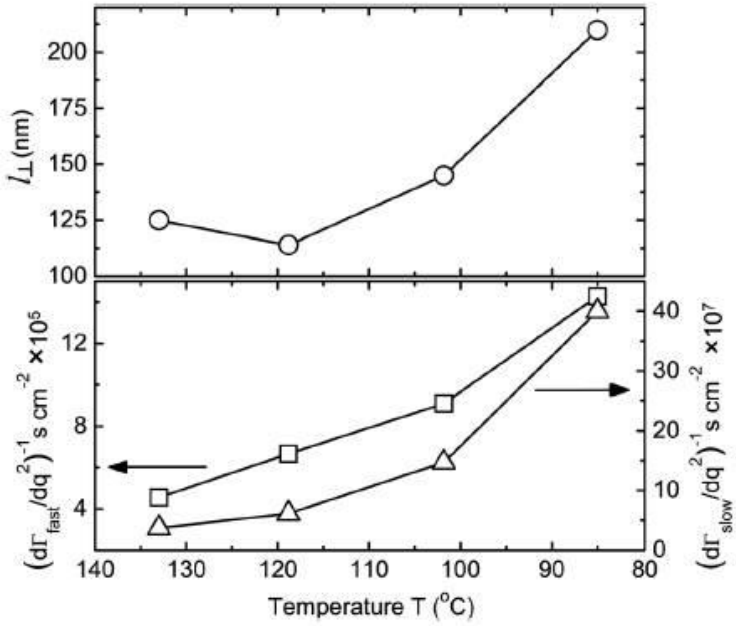

Fig. 5 Top panel: orientational correlation length for biaxial order in the uniaxial phase of DT6Py6E6, obtained from results for Γ_{fast} *vs.* q^2 and the Landau-deGennes model for the orientational free energy. Bottom panels: results for the inverse slopes $\left(\mathrm{d}\Gamma_{\text{fast}}/\mathrm{d}q^2\right)^{-1}$ and $\left(\mathrm{d}\Gamma_{\text{slow}}/\mathrm{d}q^2\right)^{-1}$, which are proportional to the viscosities for biaxial order and director fluctuations, respectively, in the uniaxial phase of DT6Py6E6.

which is due to leakage from slight imperfections (mosaic) in the homeotropic alignment and the intrinsically strong scattering cross-section associated with the uniaxial director. Thus, the correlation data were fit to the sum of three exponential decays, $g(\tau)=\left[A_{\text{fast}}\exp(-\Gamma_{\text{fast}}\tau)+A_{\text{int}}\exp(-\Gamma_{\text{int}}\tau)+A_{slow}\exp(-\Gamma_{\text{slow}}\tau)\right]^2+1$, with normalized amplitudes ($0\le A\le 1$) and relaxation rates Γ_{slow}, Γ_{int} and Γ_{fast} as fitting parameters.[36] From this analysis, we find that Γ_{int} is an order of magnitude lager than Γ_{slow} and almost one order smaller than Γ_{fast}, and that $\Gamma_{\text{slow}}\sim 10-100\,\text{s}^{-1}$ over the range of q probed. For similar q, the twist-bend fluctuations are therefore 10-100 times slower than in typical calamitic (rod-shaped) nematics, a result found previously for other BCNs.[7,37]

A representative correlation function taken in the polarized VV scattering geometry is shown at the bottom of Fig. 3. As anticipated from eqn (3) and (6), we find that the biaxial order parameter mode (Γ_{fast}) dominates the VV data for all 2θ (in particular, away from the condition $2\theta=\theta_i$). However, the "intermediate" mode, and a weak remnant of the director mode, can still be observed. As noted above, detection of the latter in a theoretically "dark" geometry may be attributed to the "leakage" effect produced by slight mosaicity in $\vec{\boldsymbol{n}}$.

Let us next consider results from the quantitative analysis of the correlation data. The dispersion (q dependence) of the relaxation rates and relative amplitudes of the three modes detected in VH scattering are shown in Fig. 4 for the 4.9 μm sample at $T_{NI}-T=33\,^{\circ}\text{C}$. Since $q_z^{\,2}\ll q_\perp^{\,2}$ for our scattering geometries, the results for the relaxation rates are plotted against $q^2=q_\perp^{\,2}=\left[2\pi\sin 2\theta\right]/\lambda^2$. They clearly demonstrate that the slow mode is hydrodynamic ($\Gamma_{\text{slow}}\to 0$ as $q\to 0$) and the fast mode is nonhydrodynamic (finite Γ_{fast} at $q=0$), and confirm their assignments to uniaxial director and biaxial order parameter fluctuations according to eqn (4) and (7), respectively. We also find that the intermediates, plotted *vs.* 2θ (bottom panel of Fig. 4), confirm the

main predictions for VH scattering described in Section II. In particular, we observe a well-defined minimum in the director mode amplitude at $2\theta = \theta_i$, and a corresponding enhancement in the nonhydrodynamic order parameter scattering. The ratio of order parameter to director amplitudes observed for the "dark uniaxial" condition is ~7:1. (The observed ratio is limited by "leakage" of the director mode, as noted above.) meanwhile, the amplitude of the intermediate mode is comparatively weak for all 2θ, except for a slight peak corresponding to $2\theta = \theta_i$.

The data for Γ_{fast} *vs.* q^2 allows an estimate of the orientational correlation length $l_\perp$ for biaxial order fluctuations. According to eqn (7) the inverse of the slope of this data divided by the intercept at $q = 0$ yields $C_\perp / a$, which in the Landau model corresponds to $l_\perp^2$. (Here the small contribution of ${q_z}^2$ is ignored.) Results for $l_\perp$ as a function of temperature are presented in Fig. 5. We see that if $l_\perp \sim 100\,\text{nm}$, which is only ~10 times lower than an optically resolvable length, and that $l_\perp$ increases with decreasing temperature.[38] As Fig. 5 also shows, the quantity $\left(\mathrm{d}\Gamma_{\text{slow}} / \mathrm{d}q^2\right)^{-1} \simeq \eta_2 (q \simeq q_\perp) / K_{22} \simeq \gamma_1 / K_{22}$, which is proportional to the director twist viscosity γ_1, increases substantially with decreasing temperature. The slope $\left(\mathrm{d}\Gamma_{\text{fast}} / \mathrm{d}q^2\right)^{-1} = \eta_\xi / C_\perp$ also increases at lower temperatures. Unfortunately, we were not able to follow the development of these parameters into the supercooled (monotropic) nematic state, because of instability in the baseline of the correlation function. The instability was a consequence of a flow-induced tilt of the homeotropic director, which was caused by temperature change and thermal contraction of the sample, and which decays back to the equilibrium, homeotropic state extremely slowly at low temperatures. The next section describes this effect in detail.

V. Result: optical conoscopy, FCPM, and CARS

Optical conoscopy was performed on homeotropic samples of DT6Py6E6 in both the enantiotropic and monotropic regions of the nematic phase. In equilibrium at a fixed temperature, the conoscopic patterns consisted of two straight, crossed isogyres, a signature of optical uniaxility. However, as Fig. 6a and b show for a $13\,\mu\text{m}$ thick sample, a transient change in conoscopic pattern occurs while the temperature is changing (in either heating or cooling), and is most striking in the monotropic range. The data are recorded during and after 5° steps in temperature at a rate of $1^\circ\text{C}\,\text{min}^{-1}$. Fig. 6c and d display the corresponding change in transmission of 633 nm laser light through the sample placed between crossed polarizers. During the temperature change, the sample shows both an increase in light transmission and a separation of the initially crossed isogyres; after a certain, temperature-dependent time interval τ_r, both effects relax back to the initial, uniaxial condition. The relaxation time τ_r strongly depends on conditions such as the cell thickness, initial temperature, and rate of temperature change. We determined the qualitative relationship among these parameters to be the following: τ_r (and the degree of isogyre splitting) increase with increasing cell thickness and rate of temperature change, and decrease at higher initial temperatures. The transient splitting of isogyres was observed for temperatures $T_{\text{NI}} - T$ from $\leq 35\,^\circ\text{C}$ to $120\,^\circ\text{C}$; over this range, the separation of isogyres increases somewhat from higher to lower T, while τ_r varies enormously, from ~1 s to ~10 h.[39]

The effects demonstrated in Fig. 6 could depend on a spatial gradient in temperature across the field of observation, as well as on its temporal rate of change. Since the thermal conductivity of a nematic is anisotropic,

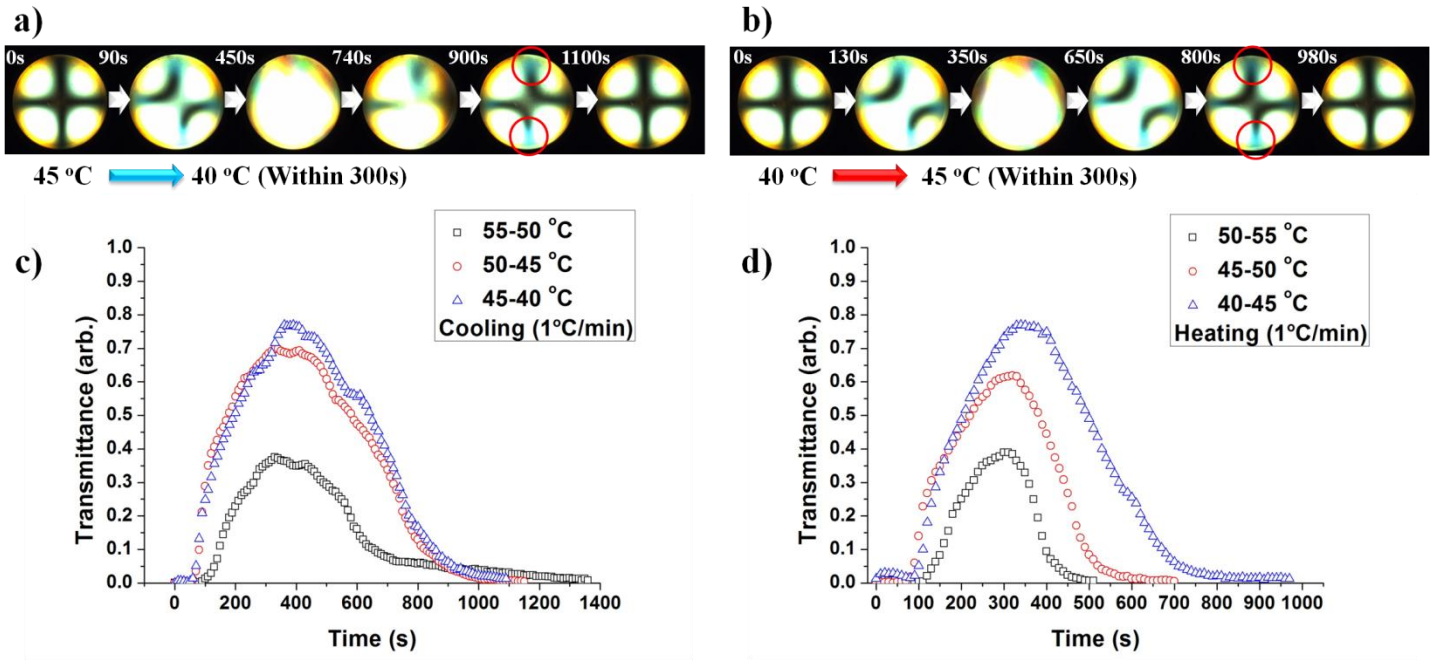

Fig. 6 Top: changes in the conoscopic pattern with time while (a) cooling and (b) heating a 13 μm thick homeotropic sample of DT6Py6E6. Bottom: data for the intensity of 633 nm light transmitted through the homeotropic sample placed between crossed polarizers, as a function of time, following the temperature changes indicated in (c) cooling and (d) heating.

thermal gradients may cause a realignment of the optical axis.[40-42] For a homeotropic sample, this would correspond to a tilting of the director away from the cell normal. In a typical hot stage, a temperature variation across the sample plane is unavoidable because of the presence of the transparent window necessary for optical observation. We conducted a separate experiment to demonstrate that for the data in Fig. 6, the effect of spatial gradients is insignificant compared to the variation of temperature with time. In order to establish a fixed thermal gradient, a homeotropic sample was placed as a bridge between a cold plate kept at $52\,^{o}C$ and a separate hot plate at $91\,^{o}C$ (Fig. 7). The temperature of each plate was precisely regulated by a combination of a ceramic heating element and a refrigerated circulating water bath. As the gap between two plates was varied between 1 and 8 mm, we observed that the conoscopic texture in the middle of the cell always maintained the feature (fourfold symmetric cross pattern) of a uniaxial, homeotropically nematic.

We next performed a series of experiments that clearly demonstrate an expansion/contraction of DT6Py6E6 with changes in temperature, and a concomitant flow-induced director tilt that varies with the rate of temperature change. Fig. 8 shows the thermal expansion and shrinkage in a homeotropic sample produced by changing the temperature from $120\,^{o}C$ to $40\,^{o}C$ and back to $120\,^{o}C$ at a rate of $1\,^{o}C\,min^{-1}$. The expansion and shrinkage are seen as a motion of the meniscus line at the LC-air interface in the cell. We independently determined the coefficient α_V of thermal expansion by injecting the liquid crystal into a cylindrical quartz capillary (diameter 320 μm), and recording the displacement of the meniscus as a function of temperature. We obtained the value $\alpha_V = 19\times10^{-4}\,per\,^{o}C$. For comparison, we measured α_V in the standard clamitic liquid crystal 5CB and found $\alpha_V = 6.0\times10^{-4}\,per\,^{o}C$; thus, α_V is significantly larger in DT6Py6E6 than in a conventional calamitic nematic.

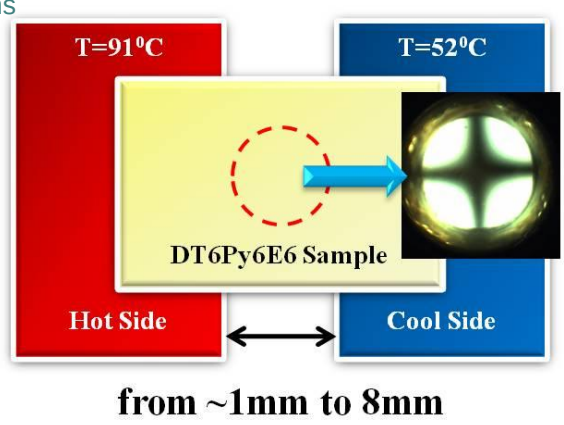

Fig. 7 Schematic of the technique used to produce a thermal gradient in plane of a homeotropically aligned sample of DT6Py6E6 in the nematic phase The inset shows the corresponding stationary conoscopic pattern, indicating a steady uniaxial state when the gap between hot and cold plates was varies as shown.

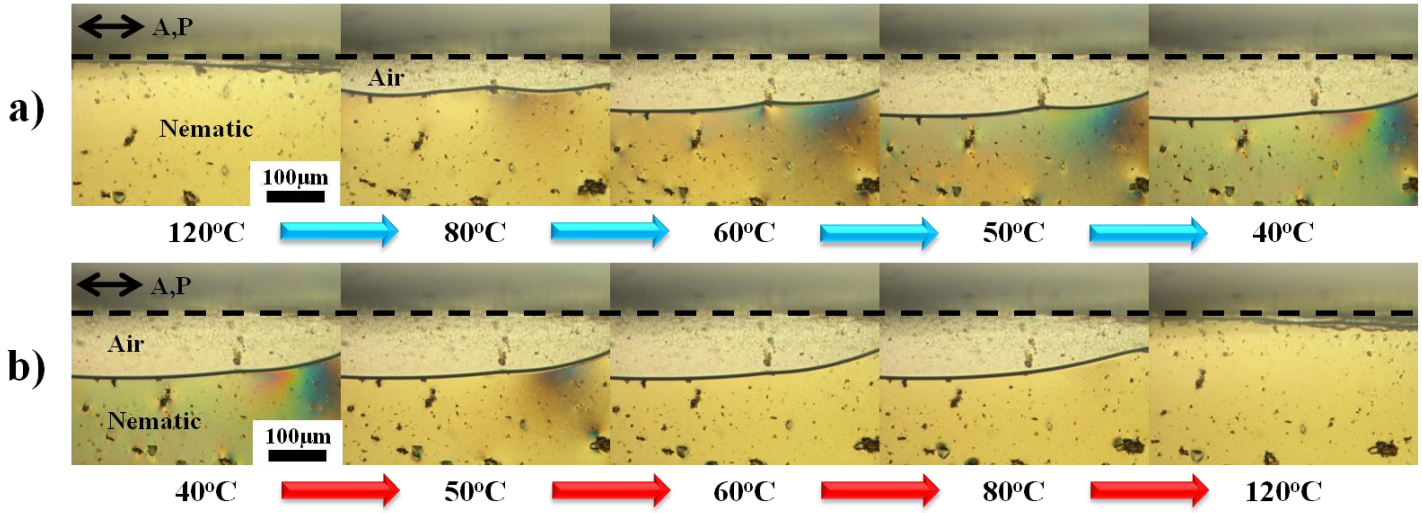

Fig. 8 Thermal shrinkage and expansion of a 13 μm thick homeotropic sample of DT6Py6E6 during (a) cooling and (b) heating, as visualized by the displacement of the meniscus near the edge of cell observed under the polarizing microscope with parallel polarizers. The dotted black line indicates the edge of the top plate covering the LC layer.

The thermal expansion and shrinkage induce flows in the sample, which we verified by observing the motion of small fluorescent spheres of diameter 0.19 μm added at a concentration of <1% (by volume) to the liquid crystal in 20 μm thick homeotropic cells. In particular, we used FCPM to show that a change of temperature is accompanied by a displacement of particles in the cell. Fig. 9 displays typical results. Once the temperature is stabilized, the particles stop moving. The direction of particle displacement correlates with the direction of movement of the air-liquid crystal interface in Fig. 8. The particle motion thus reveals that there is a material flow in the bulk of the cell, along the direction of sample contraction/expansion. At lower temperatures, the displacements of the particles become larger (for the same rate of temperature change). In liquid crystals, material flows are able to realign the director.[33] By simply pushing against the cell substrate, we demonstrated (fig. 10) that an in-plane flow in a homeotropic cell of DT6Py6E6 can generate a splitting of isogyres similar to that observed in Fig. 6.

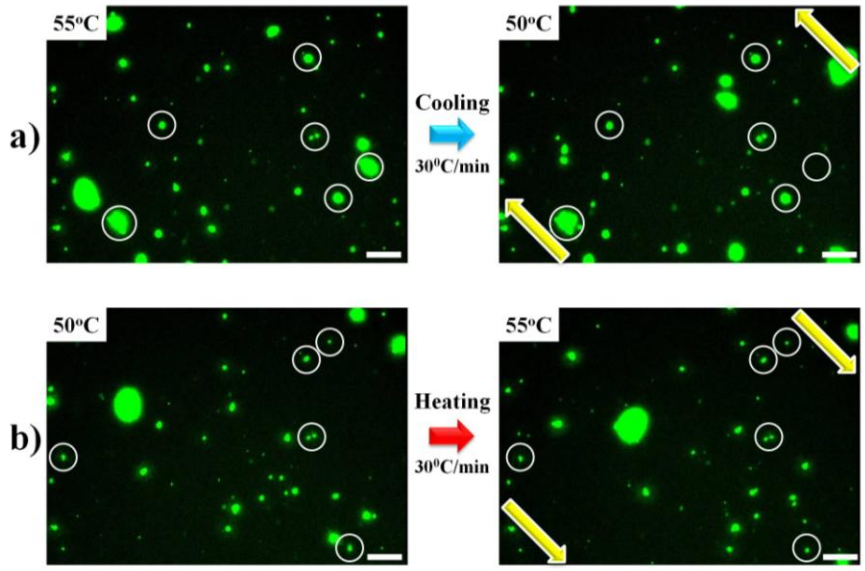

Fig. 9 Movement of fluorescent particles in a homeotropic sample of DT6Py6E6 observed by FCPM on (a) cooling and (b) heating the sample. Black area is the LC (no fluorescent intensity) and green dots are the fluorescent particles suspended in the LC. Arrows indicate the direction of particle motion. The particles in the solid circle are fixed by adhesion to the cell surfaces. Scale bar (bottom right corner in each image) is 50 μm.

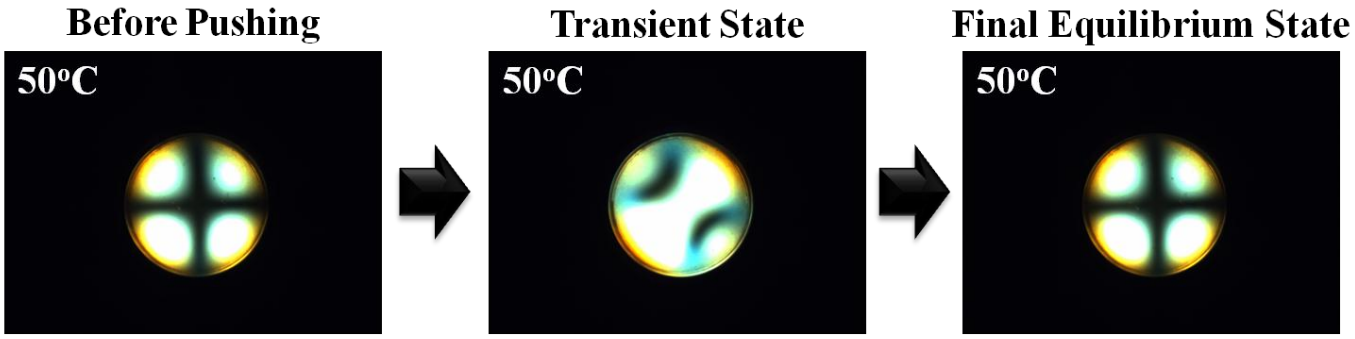

Fig. 10 Splitting of conoscopic isogyres caused by material flow after pushing on the surfaces of a cell containing a 20 μm layer of homeotropically aligned DT6Py6E6.

We now turn to additional results, which confirm that during a temperature change, the uniaxial director tilts away from the equilibrium direction perpendicular to the glass plates in the homeotropic cell. In the first experiment, the director tilt was visualized by FCPM with a polarized probe beam. Pure DT6Py6E6 was doped with a tiny amount (0.01 wt%) of a fluorescent dye $N,N'-$bis(2,6-dimethylphenyl)-3,4,9,10-perylenetetracarboxylic diimide (BTBP, Sigma-Aldrich). A separate, homogeneous planar sample was prepared to establish that the transition dipole $\vec{\boldsymbol{d}}$ of BTBP is parallel to the uniaxial director $\vec{\boldsymbol{n}}$ of DT6Py6E6, similarly to a procedure described elsewhere.[43,44] The FCPM textures record the fluorescent light intensity of a sample that depends on the angle α between the linear polarization of the probing light and the transition dipole of BTBP dye molecules and thus the director, as the two are parallel to each other. Specifically the fluorescent intensity depends on α as $I_{\mathrm{FCPM}} \propto \cos^4 \alpha$. Fig. 11 shows a sequence of FCPM images for a 13 μm thick homeotropic cell. In all cases, the probing light impinges normally onto the horizontal cell. For homeotropic alignment, the probing light polarization is perpendicular to the director, $\alpha = \pi/2$ and the FCPM texture is dark, I_{FCPM} is

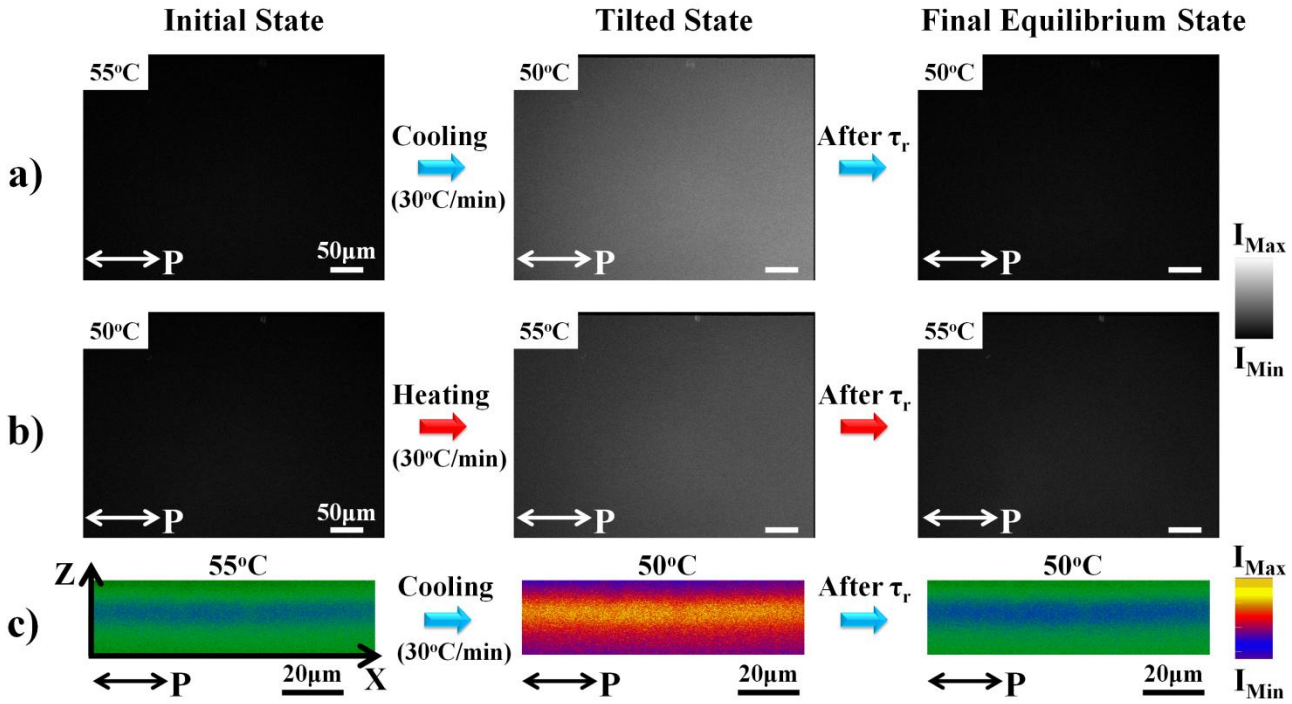

Fig. 11 FCPM textures of a 13 μm thick homeotropic sample of DT6Py6E6 doped with 0.01 wt% of the fluorescent dye BTBP. (a) and (b): In-plane ($X-Y$) textures. (c): Vertical optical slices ($X-Z$ scans). *P* indicates the polarizer axis.

close to zero (orientational fluctuations always yield some non-zero contribution to I_{FCPM} even in the perfect homeotropic state), as seen for the equilibrium states at fixed temperatures 50 °C and 55 °C. The textural appearance is fully compatible with the uniaxial homeotropic structure in which $\vec{d}$ and $\vec{n}$ are both perpendicular to the plane of the cell. However, in the transient regime (during and immediately after a 5 °C temperature steps), the FCPM textures become bright as seen in the top view of the cell (Fig. 11a and b) and in the vertical optical cross-section of the cell (Fig. 11c). A strong increase in the intensity I_{FCPM} of fluorescent light indicates that $\vec{n}$ is temporarily tilted away from the normal to the cell, so that α is different from $\pi/2$.

As an additional confirmation that temperature variation induces a tilting of $\vec{n}$, we employed the label-free technique of coherent anti-Stokes Raman Scattering (CARS) microscopy[45,46] to probe directly the orientation of pre-selected chemical bonds in the liquid crystalline phases.[47,48] In CARS microscopy, the light collected to form an image is generated from a nonlinear four wave mixing process, when the beating frequency of the two overlapping probing laser beams matches the frequency of a specifically selected molecular vibrational mode in the sample. If the direction of the selected chemical bond is orthogonal to the polarization of two probing beams, the CARS signal is minimum, if the two are parallel, the signal is maximum. In our set-up (described in fuller detail in ref. 47), we use a passively mode-locked Nd:YVO4 oscillator (High Q Laser, PicoTrain) which delivers 6 ps pulses at 1064 and 532 nm at a repetition rate of 80 MHz The 532 nm light is used to synchronously pump an optical parametric oscillator (APE GmbH, Levante Emerald) based on a non-critically phase-matched lithium triborate (LBO) crystal. The output wavelength of the OPO is tunable from 680-980 nm by adjusting the LBO temperature, and is used as the pump wavelength for CARS. The idler wave is rejected with a short pass filter (Chroma Technology, 985SP). The signal beam is then combined with the 1064 nm

fundamental from the Nd:YVO4 laser *via* a dichroic mirror (Chroma Technology, 1064DCRB). The linear polarization of the combined beams can be rotated using an achromatic zero order half-wave plate (Thorlabs, AHWP05M-950) placed in the beam path, and the beams may be attenuated to the desired power levels using a variable neutral density filter. The beams were coupled into a modified laser scanning microscope (Olympus, FV300-IX71) and focused onto the sample. The anti-Stokes light emitted from the sample was then detected in a backward direction by an epi-detector.

Fig. 12a shows a portion of the Raman spectrum of DT6Py6E6, from which we identify the peak corresponding to the carbon-carbon triple bond at 2207 cm^{-1}.[49] This bond was selected to trace the orientation of DT6Py6E6 molecules in the sample during the temperature changes. Because it is rigid, there is no bending of the bond that could degrade the fidelity of CARS images. We used low power (0.1 W) irradiation to prevent damage to the sample. In order to establish how the CARS signal intensity depends on the orientation of preselected chemical bonds with respect to the direction of linear polarization P_{CARS} of the probing (pump and Stokes) laser beams, we first examined homogeneous planar cells of thickness 20 μm, filled with either a standard calamitic nematic, pentylcyanobiphenyl (5CB), or with DT6Py6E6. For 5CB, we collected the CARS signal at the frequency 2223 cm^{-1}, corresponding to vibrations of the $C \equiv N$ triple bond.

The CARS intensity from the planar sample of 5CB is presented in Fig. 12b as a function of the angle ϕ_{CARS} between the rubbing direction (equivalently, the director $\vec{n}$) and the polarization direction P_{CARS}. The $C \equiv N$ bond is parallel to the long axis of the 5CB molecule and therefore, on average, to $\vec{n}$. As a result, $\cos\phi_{CARS} = P_{CARS} \cdot \vec{n}$ and the CARS signal reaches a pronounced maximum when P_{CARS} is parallel to the rubbing

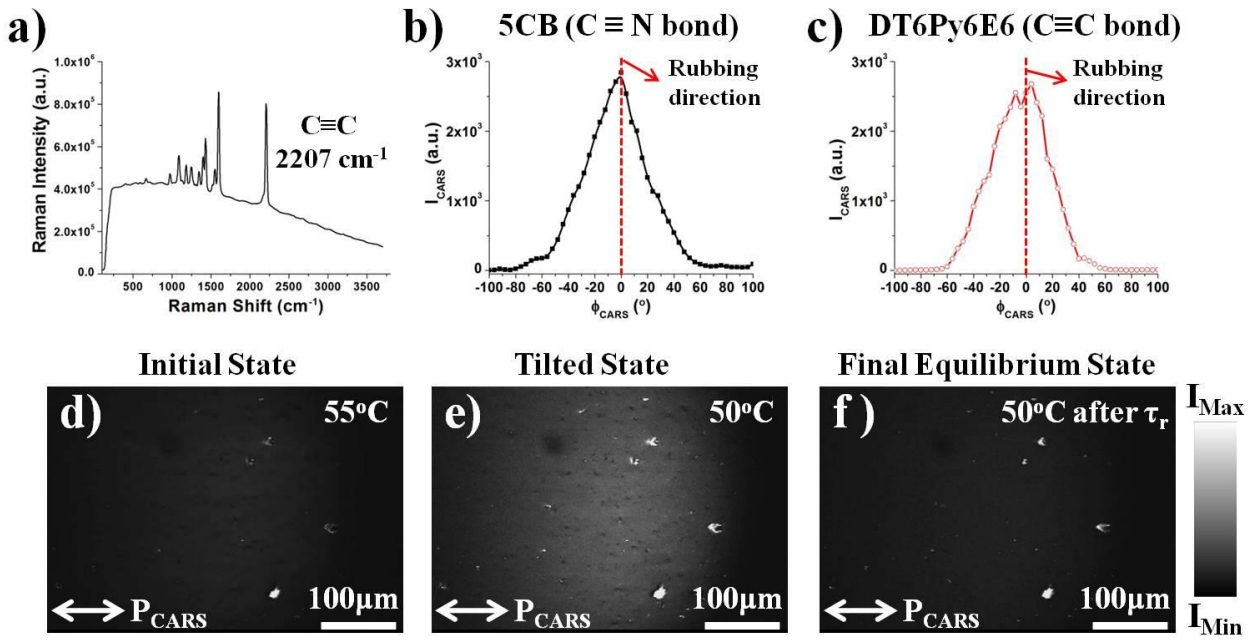

Fig. 12 (a) Raman spectrum of DT6Py6E6. (b) CARS signal intensity in a homogeneous planar cell of the standard calamitic nematic 5CB as a function of the angle ϕ_{CARS} measured between the rubbing direction and polarization of probing beams. (c) CARS signal intensity as a function of ϕ_{CARS} in a homogeneous planar cell of DT6Py6E6. (d-f) Epi-detected CARS texture in a 20 μm thick homeotropic DT6Py6E6 sample, stabilized at 55 °C (d), at 50 °C (f), and during temperature change (transient state) between 55 and 50 °C (e). Note darker field in (d) and (f), and a brighter field in (e). P_{CARS} indicates the polarization direction of the probing laser beams.

direction, $\phi_{CARS} = 0^o$, and decreases sharply when $|\phi_{CARS}|$ decreases to about 60^o. In the range $60^o < |\phi_{CARS}| < 90^o$, the CARS signal intensity shows a very weak angular dependence. This behavior is expected for the illumination geometry used, as the electric fields $\vec{E}_P$ of the pump and $\vec{E}_S$ of the Stokes beams are parallel to each other, so that one expects $I_{CARS} \propto \left(\chi^{(3)} E_P{}^2 E_S\right)^2 \propto \cos^6 \phi_{CARS}$, where $\chi^{(3)}$ is the third-order susceptibility.[47,50] The calculated angular dependence of I_{CARS} provides a satisfactory fit of the experimental data in Fig. 12b.

In DT6Py6E6, the carbon-carbon triple bonds are tilted with respect to the long axis of the molecule, by about 10^o (Fig. 1), and thus tilted with respect to the director. This feature is clearly reflected in the angular dependency of the CARS signal measured for the planar cell, Fig. 12c. The signal intensity I_{CARS} shows two local peaks, shifted to the right and to the left by a few degrees from the rubbing axis, where $\phi_{CARS} = 0^o$. As in the case of 5CB, the signal rapidly decreases as $|\phi_{CARS}|$ increases to approximately 60^o, and then depends only weakly on $|\phi_{CARS}|$ between 60^o and 90^o.

We now consider the CARS data for a homeotropically aligned 20 μm sample of DT6Py6E6. Fig. 12d-f show the sequence of CARS images obtained during a temperature change from $55\,^oC$ to $50\,^oC$. In the initial state, thermally stabilized at $55\,^oC$, the texture is dark, as the angle between the polarization of the probing beams and the $C \equiv C$ bonds is around 80^o for the homeotropic sample (as noted previously, the bonds are tilted by $\sim 10^o$ with respect to the director, which is now perpendicular to the plane of incidence). When the temperature is quickly reduced to $50\,^oC$, the signal increases, and the texture becomes bright, Fig. 12e, indicating tilt of the $C \equiv C$ bonds away from the cell normal and toward the direction of P_{CARS}. Using the data in Fig. 12c, the average angle between the bond direction and the horizontal plane in Fig. 12e is estimated to be in the range $45^o < |\phi_{CARS}| < 60^o$. This tilt of the molecules is transient. Once the temperature is stabilized at $50\,^oC$, the texture relaxes back to the dark state in ~30 min, indicating that the angle between the $C \equiv C$ bonds and P_{CARS} returns to the initial value for the homeotropic state (compare Fig. 12d and f). The CARS observations thus demonstrate a transient tilt of the DT6Py6E6 molecules, in agreement with the data obtained by FCPM (Fig. 11).

The spatial resolution of FCPM and CARS is not sufficient to establish the details of the vertical profile of the director field in the transient regime in DT6Py6E6 cells. However, the nature of the isogyre split in the conoscopic image indicates that the director is tilted in a bow-type pattern that was previously documented in studies of homeotropic cells filled with uniaxial nematics and subject to the pressure-gradient-induced Poiseuille flow.[51] The flow-imposed realigning torque on the director is proportional to the shear rate $\gamma \propto \partial v_x / \partial z$. (Here v_x is the velocity component in the plane of the cell and z is the direction normal to the cell plane.) The shear rate γ vanishes at the cell surfaces, $z = 0, d$, and also in the midplane, $z = d/2$, where the gradient of velocity is zero. The director thus remains perpendicular to the bounding plates at the positions $z = 0, d, d/2$, and is tilted in two opposite directions in the regions $0 < z < d/2$ and $d/2 < z < d$. In the conoscopic observations, this is equivalent to two tilted domains of the uniaxial nematic that are placed on top of each other, producing a pattern of split isogyres that resembles-misleadingly so-the texture of a biaxial monodomain. We recently verified[52] that the very same effect is observed when homeotropically aligned liquid

crystals composed of ordinary rodlike molecules, including well-known compounds such as 5CB, E7, MLC-6815, and ZLI-2806, are subjected to a temperature change.

The transient director tit detected in DT6Py6E6 should not be confused with the surface anchoring transition observed as a function of temperature in other homeotropically aligned bent-core materials.[14,15] In the latter cases, the director establishes and equilibrium tilted configuration that does not change with time, as long as the temperature remains fixed. By contrast, in the case of DT6Py6E6, the tilt is an out-of-equilibrium feature that is observed only during a finite time interval that depends on the rate of temperature change. Although both effects mimic rather closely optical features expected for a biaxial nematic sample, their natures are very different from each other and from a true thermodynamic biaxial state. It is also worth noting a very recent report on the appearance of a secondary Schlieren texture upon temperature change in an unaligned BCN,[53] which was considered as an indication of biaxiality. It would be of interest to explore whether this effect is related to the finite rate of temperature change, *i.e.*, represents an effect similar to the one described above for homeotropically aligned DT6Py6E6.

VI. Discussion

As suggested in the Introduction, our experimental results can be explained by a model for the small-scale structure of the nematic phase, which is based on the formation of short-range biaxial complexes among DT6Py6E6 molecules. An analysis of the SAXS data in ref. 26 led the authors to propose the biaxial configuration of molecules shown in Fig. 13. We suppose that the average density of such DT6Py6E6 complexes is temperature-dependent. (Their average size could also depend on T, but our data indicate that the complexes remain nanoscale entities throughout the nematic.) A significant increase in their number density as the temperature is reduced (specifically from the enantiotropic to monotropic regime)- and therefore a concomitant increase in the packing density of molecules- would produce a contraction of the sample on cooling (or expansion while heating), initiating the flow-induced director tilt we observed. The SAXS data in ref. 26 reveal a marked increase in the X-ray intensity, in the monotropic temperature range, at wavevectors corresponding to the lateral pairing of molecules indicated in Fig. 13. This is consistent with an increasing density of molecular complexes.

At higher temperatures in the nematic phase, a diffusion of the biaxial complexes could give rise to orientational order parameter fluctuations, as observed in our light scattering, in a natural way. In particular, thermal molecular diffusion provides a pathway to concentration fluctuations of the complexes; where the concentration becomes high, a spontaneous local ordering of the secondary optical axis $\hat{m}$ (indicated in Fig. 13) may occur. This yields a nonhydrodynamic order parameter mode that scatters light into both polarized and depolarized channels (Fig. 3). Note that even a fairly large orientational correlation length (estimated from Fig. 4 at ~100 nm) does not imply a comparable length for *mass density* correlations (the SAXS results show the latter remain of the order a few molecular spacings).

The proposed model additionally accounts for the origin of the intermediate, hydrodynamic mode detected in our correlation data. From Fig. 4, we obtain $\Gamma_{\text{int}}/q^2 = 6\times10^{-7}\,\text{s}^{-1}\text{cm}^2$ at $T_{\text{NI}} - T = 33\,^{\circ}\text{C}$. If, as suggested above, the order parameter fluctuations are coupled to translational diffusion of individual molecules in the regions between the complexes, then a diffusion mode should show up (weakly) in both polarized and depolarized scattering, with a value of Γ/q^2 comparable to a molecular diffusion constant D. Typical values for thermotropic nematics, $D \sim 10^{-7} - 10^{-6}\,\text{s}^{-1}\text{cm}^2$,[54] compare favorable to the experimental result for Γ_{int}/q^2.

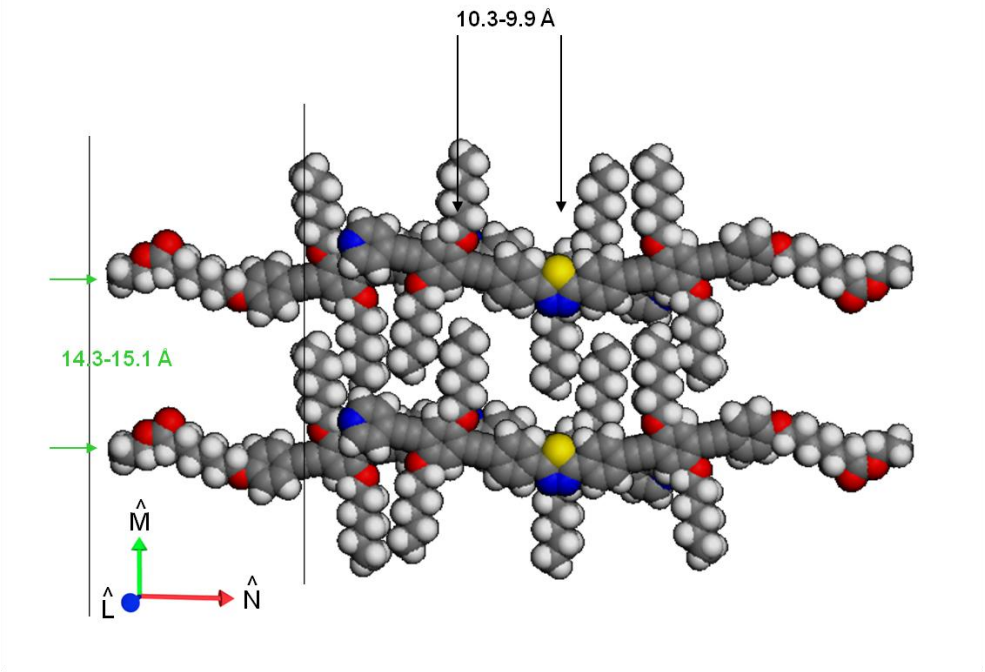

Fig. 13 Schematic of short-range order between DT6Py6E6 molecules in the nematic phase, as inferred from small angle X-ray scattering measurements.[26] Note that the orientational order within the four molecule "complex" shown is biaxial.

As we have already pointed out, the slower (and strongly scattering) hydrodynamic mode detected in depolarized scattering is certainly associated with the uniaxial director. In a separate study,[55] we confirmed that the orientational viscosities for $\hat{\boldsymbol{n}}$ director rotations in DT6Py6E6 are much larger than ordinary thermotropic nematics; this is likely a consequence of both the complexing of molecules as well as enhanced entanglements due to the multiple chain substitutions on the DT6Py6E6 molecule. For this same reason, we expect the activation energy for director rotations to be significantly higher than in ordinary calamitics, accounting for the large and temperature-dependent values of the tilt relaxation time τ_r recorded in Fig. 6.

Some issues in the details of the proposed model need to be further addressed. For example, it is not completely clear why the molecular diffusion constant D could be in the normal range (at least as assumed in the above discussion of the intermediate mode), while the orientational $(\hat{\boldsymbol{n}})$ viscosities are quite large. There may also appear to be some difficulty with the notion that biaxial complexes persist in equilibrium in a uniaxial system made up of one molecular species. However, it may be that the system is not in a true equilibrium state; indeed, at low temperature, the nematic phase is monotropic, and the material crystallizes for temperatures below $\sim 50\,^{o}$C within a matter of hours. Alternatively, the theory described in ref. 31 predicts a possible intermediate nematic state that if macroscopically uniaxial but contains microscopic biaxial domains.

VII. Conclusion

We found that a shape persistent, bent-core liquid crystal, with a broad nematic range, exhibits both significant biaxiality fluctuations and a remarkable flow-induced, transient realignment of the uniaxial director, which is triggered by a temperature change and stems from a large thermal expansivity. We suggested that these phenomena have a common origin: the temperature-dependent formation of nanoscale, biaxial complexes of

molecules, which are distinct from the relatively temperature-insensitive smectic-C-type clustering recently observed in other bent-core nematics. Although the specific compound we studied does not exhibit stable biaxiality, the design strategy based on shape-persistent core structure is certainly worth pursuing toward that still elusive goal in thermotropic nematic liquid crystals.

Acknowledgements

MM and SS are grateful to D. W. Allender for several useful conversations, and also acknowledge funding from the US Department of Energy under grant DE-SC0001412, which supported the light scattering studies. AJ and JG thank the NSF for support under grant DMR-0964765. The FCPM and CARS studies by YKK, BS, LT, and ODL were supported by the US DOE under grant DE-FG02-06ER46331. YKK and ODL also acknowledge Samsung Electronics Corporation for financial support. ML and JS thank the Deutsche Forschungsgemeinschaft for support under grant LE1571/2-1.

References

1 M. J. Freiser, *Phys. Rev. Lett.*, 1970, **24**, 1041-1043.
2 B. R. Acharya, A. Primak and S. Kumar, *Phys. Rev. Lett.*, 2004, **92**, 145506; B. R. Acharya, S. –W. Kang and S. Kumar, *Liq. Cryst.*, 2008, **35**, 109-118; B. R. Acharya, S. –W. Kang, V. Prasad and S. Kumar, *J. Phys. Chem. B*, 2009, **113**, 3845-3852.
3 L. A. Madsen, T. J. Digemans, M. Nakata and E. T. Samulski, *Phys. Rev. Lett.*, 2004, **92**, 145505.
4 C. D. Southern, P. D. Brimicombe, S. D. Siemianowski, S. Jaradat, N. Roberts, V. Gortz, J. W. Goodby and H. F. Gleeson, *Europhys. Lett.*, 2008, **28**, 56001; Y. Xiang, J. W. Goodby, V. Gortz and H. F. Gleeson, *Appl. Phys. Lett.*, 2009, **94**, 193507.
5 M. S. Park, B. -J. Yoon, J. O. Park, V. Prasad, S. Kumar and M. Srinivasarao, *Phys. Rev. Lett.*, 2010, **105**, 027801.
6 H. G. Yoon, S. W. Kang, R. Y. Dong, A. Marini, K. A. Suresh, M. Srinivasarao and S. Kumar, *Phys. Rev. E*: *Stat., Nonlinear, Soft Matter Phys.*, 2010, **81**, 051706.
7 J. Olivares, S. Stojadinovic, T. Dingemans, S. Sprunt and A. Jakli, *Phys. Rev. E: Stat. Phys., Plasmas, Fluids, Relat. Interdiscip. Top.*, 2003, **68**, 041704.
8 S. Stojadinovic, A. Adorjan, S. Sprunt, H. Sawade and A. Jakli, *Phys. Rev. E: Stat., Nonlinear, Soft Matter Phys.*, 2002, **66**, 060701 (**R)**.
9 N. Vaupotic, J. Szydlowska, M. Salamonczyk, A. Kovarova, J. Svoboda, M. Osipov, D. Pociecha and E. Gorecka, *Phys. Rev. E: Stat., Nonlinear, Soft Matter Phys.*, 2009, **80**, 030701.
10 O. Francesangeli, V. Stanic, S. I. Torgova, A. Strigazzi, N. Scaramuzza, C. Ferrero, I. P. Dolbnya, T. M. Weiss, R. Berardi, L. Muccioli, S. Orlandi and C. Zannoni, *Adv. Funct. Mater.*, 2009, **19**, 2592-2600.
11 C. Keith, A. Lehmann, U. Baumeister, M. Prehm and C. Tschierske, *Soft Matter*, 2010, **6**, 1704-1721.
12 S. H. Hong, R. Verduzco, J. C. Williams, R. J. Twieg, E. DiMasi, R. Pindak, A. Jakli, J. T. Gleeson and S. Sprunt, *Soft Matter*, 2010, **6**, 4819-4827.
13 K. van Le, M. Mathews, M. Chambers, J. Harden, Q. Li, H. Takezoe and A. Jakli, *Phys. Rev. E: Stat., Nonlinear, Soft Matter Phys.*, 2009, **79**, 030701.
14 B. Senyuk, H. Wonderly, M. Mathes, Q. Li, S. V. Shiyanovskii and O. D. Lavrentovich, *Phys. Rev. E: Stat., Nonlinear, Soft Matter Phys.*, 2010, **82**, 041711.

15 B. Senyuk, Y. –K. Kim, L. Tortora, S. –T. Shin, S. V. Shiyanovskii and O. D. Lavrentovich, *Mol. Cryst. Liq. Cryst.*, 2011, **540**, 20-41.
16 J. H. Lee, T. K. Lim, W. T. Kim and J. I. Jin, *J. Appl. Phys.*, 2007, **101**, 034105.
17 J. H. Lee, T. K. Lim and T. H. Yoon, *Phys. Rev. E: Stat., Nonlinear, Soft Matter Phys.*, **83**, 051705.
18 J. You, J. Y. Jung, K. Rhie, V. M. Pergamenshchik and S. T. Shin, *J. Korean Phys. Soc.*, 2008, **52**, 342-349.
19 G. R. Luckhurst, *Thin Solid Films,* 2001, **393**, 40-52.
20 G. R. Luckhurst, *Nature,* 2004, **430**, 413.
21 C. Chiccoli, I. Feruli, O. D. Lavrentovich, P. Pasini, S. V. Shiyanovskii and C. Zannoni, *Phys. Rev. E: Stat., Plasmas, Fluids, Relat. Interdiscip. Top.*, 2002, **66**, 030701.
22 K. Severing and K. Saalwachter, *Phys. Rev. Lett.*, 2004, **92**, 125501.
23 R. Stannarius, *J. Appl. Phys.*, 2008, **104**, 036104.
24 Y. Jang, V. Panov, A. Kocot, J. K. Vij, A. Lehmann and C. Tschierske, *Appl. Phys. Lett.*, 2009, **95**, 183304.
25 R. Y. Dong and A. Marini, *J. Phys. Chem. B*, 2009, **113,** 14062-14072.
26 J. Seltmann, A. Marini, B. Mennucci, S. Dey, S. Kumar and M. Lehmann, *Chem, Mater.*, 2011, **23**, 2630-2636.
27 M. Lehmann, *Liq. Cryst.*, 2011, **38**, 1389-1405.
28 J. Harden, B. Mbanga, N. Eber, K. Fodor-Csorba, S. Sprunt, J. T. Gleeson and A. Jakli, *Phys. Rev. Lett.*, 2066, **97**, 157802.
29 C. Bailey, K. Fodor-Csorba, J. T. Gleeson, S. Sprunt and A. Jakli, *Soft Matter,* 2009, **5**, 3618-3622.
30 C. Bailey, K. Fodor-Csorba, R. Verduzco, J. T. Gleeson, S. Sprunt and A. Jakli, *Phys. Rev. Lett.,* 2009, **103**, 237803.
31 A. G. Vanakaras and D. J. Photinos, *J. Chem. Phys.*, 2008, **128**, 154512; S. D. Peroukidis, P. K. Karahaliou, A. G. Vanakaras and D. J. Photinos, *Liq. Cryst.*, 2009, **36**, 727-737.
32 A. De Vries, *Mol. Cryst. Liq. Cryst.*, 1970, **10**, 219-236; A. de Vries, *J. Phys.*, 1975, **36**, C1-1-C1-11.
33 P. G. deGennes and J. Prost, *The Physics of Liquid Crystals*, Clarendon Press, Oxford, 2nd edn, 1993, ch. 2 and 5.
34 E. A. Jacobsen and J. Swift, *Mol. Cryst. Liq. Cryst.*, 1982, **87**, 29-39.
35 The connection between the dielectric tensor of the nematic and ξ_{ij} is:[34] $\Delta\varepsilon_b\xi_{ij} = \varepsilon_{ij}{}^{\perp} - \delta_{ij}{}^{\perp}\varepsilon_{kk}{}^{\perp}/2$, and where $\varepsilon_{ij}{}^{\perp} = \delta_{ik}{}^{\perp}\varepsilon_{kl}\delta_{ij}{}^{\perp}$, $\delta_{ij}{}^{\perp} = \delta_{ij} - n_i n_j$, and n_i are components of the uniaxial director.
36 We initially attempted to fit the data to two exponential decays. Away from the condition $2\theta - \theta_i = 0$, the fits were adequate if stretched exponential forms were used, with two independent stretching exponents (thus giving the same number of parameters as a three mode analysis with pure exponentials). However, near $2\theta - \theta_i = 0$, the relaxation rate of the slower mode clearly deviates from a q^2 dependence (it jumps to a much larger value). This is clearly an unphysical result for a hydrodynamic director fluctuation mode, and indicates the contribution of an additional mode.
37 M. Majumdar, P. Salamon, A. Jakli, J. T. Gleeson and S. Sprunt, *Phys. Rev. E: Statt., Nonlinear, Soft Matter Phys.*, 2011. **83**, 031701.
38 The analysis of the our data for the nonhydrodynamic mode, leading to the estimate of $l_{\perp}$, based on a Landau-type expansion of the free energy should be valid even if the system does not exhibit a uniaxial to biaxial nematic phase transition. A low order expansion in order parameter ξ applies for small ξ fluctuations in the disordered (uniaxial) phase, even if the leading expansion coefficient has no critical temperature dependence.

39 In previous work,[26] the textures of homeotropically-aligned DT6Py6E6 samples (confined between conventional microscope slides) were studied. However, the cell thickness was not rigorously controlled. The relaxation of separated isogyres was not observed in these presumably thick cells below 50 °C, probably because the annealing time (10-15 minutes) was too short.
40 E. I. Demenev, G. A. Pozdnyakov and S. I. Trashkeev, *Tech. Phys. Lett.*, 2009, **35**, 674-677.
41 S. I. Trashkeev and A. V. Britvin, *Tech. Phys.*, 2011, **56**, 747-753.
42 M. Reznikov, B. Wall, M. A. Handschy and P. J. Bos, *J. Appl. Phys.*, 2008, **104**, 044902.
43 I. I. Smalyukh, S. V. Shiyanovskii and O. D. Lavrentovich, *Chem. Phys. Lett.*, 2001, **336**, 88-96.
44 I. I. Smalyukh and O. D. Lavrentovich, *Phys. Rev. E: Stat. Phys., Plasmas, Fluids, Relat. Interdiscip. Top.*, 2002, **66**, 051703.
45 J. X. Cheng and X. S. Xie, *J. Phys. Chem. B*, 2004, **108**, 827-840.
46 J. X. Cheng, Y. K. Jia, G. Zheng and X. S. Xie, *Biophys. J.*, 2002, **83**, 502-509.
47 B. Saar, H. S. Park, X. S. Xie and O. D. Lavrentovich, *Opt. Express*, 2007, **15**, 13585-13596.
48 A. V. Kachynski, A. N. Kuzmin, P. N. Prasad and I. I. Smalyukh, *Appl. Phys. Lett.*, 2007, **91**, 151905.
49 R. A. Meyers, *Encyclopedia of Analytical Chemistry: Applications, Theory, and Instrumentation*, John Wiley and Sons Ltd, Chichester, 2000.
50 Y. Fu, T. B. Huff, H. –W. Wnag, H. Wang and J. –X. Cheng, *Opt. Express*, 2008, **16**, 19396-19409.
51 A. D. Rey and M. M. Denn, *Annu. Rev. Fluid Mech.*, 2002, **34**, 233-266.
52 Y. –K. Kim, B. I. Senyuk and O. D. Lavrentovich, submitted.
53 S. J. Picken, T. J. Dingemans, L. A. Madsen, O. Francesangeli and E. Samulski, *Liq. Cryst.*, 2012, **39**, 19-23.
54 A. J. Leadbetter, F. P. Temme, A. Heidemann and W. S. Howells, *Chem. Phys. Lett.*, 1975, **34**, 363-368.
55 M. Majumdar, Ph.D. dissertation, Kent State University, unpublished.